JGR Atmospheres

RESEARCH ARTICLE
10.1029/2018JD030181

Relative Contributions of North and South Pacific Sea Surface Temperature Anomalies to ENSO

Ruiqiang Ding[1,2], Yu-heng Tseng[3], Jianping Li[2,4], Cheng Sun[4], Fei Xie[4], and Zhaolu Hou[1]

[1]State Key Laboratory of Numerical Modeling for Atmospheric Sciences and Geophysical Fluid Dynamics (LASG), Institute of Atmospheric Physics, Chinese Academy of Sciences, Beijing, China, [2]Laboratory for Regional Oceanography and Numerical Modeling, Qingdao National Laboratory for Marine Science and Technology, Qingdao, China, [3]Institute of Oceanography, National Taiwan University, Taipei, Taiwan, [4]College of Global Change and Earth System Sciences, Beijing Normal University, Beijing, China

Key Points:
- The extratropical North and South Pacific Oceans make comparable contributions to the development of ENSO
- The extratropical North and South Pacific precursor signals may be used together to better predict the ENSO events

Correspondence to:
R. Ding,
drq@mail.iap.ac.cn

Citation:
Ding, R., Tseng, Y.-h., Li, J., Sun, C., Xie, F., & Hou, Z. (2019). Relative contributions of North and South Pacific sea surface temperature anomalies to ENSO. *Journal of Geophysical Research: Atmospheres*, *124*, 6222–6237. https://doi.org/10.1029/2018JD030181

Received 16 DEC 2018
Accepted 10 MAY 2019
Accepted article online 29 MAY 2019
Published online 21 JUN 2019

Author Contributions:
Conceptualization: Ruiqiang Ding
Methodology: Ruiqiang Ding, Yu-heng Tseng, Cheng Sun, Zhaolu Hou
Software: Yu-heng Tseng, Cheng Sun, Fei Xie, Zhaolu Hou
Validation: Fei Xie
Visualization: Zhaolu Hou
Writing - original draft: Ruiqiang Ding
Writing – review & editing: Yu-heng Tseng, Jianping Li

Abstract Variations in the sea surface temperature (SST) field in both the North Pacific (represented by the Victoria mode [VM]) and the South Pacific (represented by the South Pacific quadrapole [SPQ] mode) are related to the state of the El Niño–Southern Oscillation (ENSO) three seasons later. Here with the aid of observational data and numerical experiments, we demonstrate that both VM and SPQ SST forcing can influence the development of ENSO events through a similar air-sea coupling mechanism. By comparing ENSO amplitudes induced by the VM and SPQ, as well as the percentages of strong ENSO events followed by the VM and SPQ events, we find that the VM and SPQ make comparable contributions and therefore have similar levels of importance to ENSO. Additional analysis indicates that although VM or SPQ SST forcing alone may serve as a good predictor for ENSO events, it is more effective to consider their combined influence. A prediction model based on both VM and SPQ indices is developed, which is capable of yielding skillful forecasts for ENSO at lead times of three seasons.

1. Introduction

The El Niño–Southern Oscillation (ENSO) is the most dominant climate fluctuation in the tropical Pacific at seasonal-to-interannual time scales. It has significant impacts on global weather and climate variability through changing the tropical Pacific convection patterns that excite poleward-propagating atmospheric Rossby waves (Alexander et al., 2002). The development of ENSO events is attributed to a positive feedback known as the Bjerknes feedback (Bjerknes, 1969), which involves an unstable interaction between the intensity of the trade winds and zonal contrasts in sea surface temperature (SST) associated with changes in the ocean thermocline depth. Despite the fact that significant advances have been made in our understanding of ENSO over the past few decades, the mechanism behind the initiation of the Bjerknes feedback remains the subject of considerable debate.

Studies have suggested that some tropical phenomena, such as the Madden-Julian oscillation (Madden & Julian, 1994) and Westerly Wind Events (McPhaden, 1999; McPhaden et al., 1992), may play an important role in triggering the Bjerknes feedback. In addition, there is increasing observational and model evidence supporting the possible role of extratropical oceans in the onset of ENSO (e.g., Ballester et al., 2011; Boschat et al., 2013; Ding, Li, Tseng, Sun, et al., 2015; Ding, Li, & Tseng, 2015; Ham et al., 2013; Jin & Kirtman, 2009; Terray, 2011; Vimont, Wallace, et al., 2003; Wang et al., 2012). In particular, studies have identified a possible forcing of ENSO by the extratropical North Pacific Ocean (Anderson, 2004; Boschat et al., 2013; Ding, Li, Tseng, Sun, et al., 2015, 2017; Tseng, Ding, et al., 2017; Vimont, Wallace, et al., 2003; Vimont, Battisti, et al., 2003; Wang et al., 2012, 2013). These studies explored the possible influence of the North Pacific Oscillation (NPO; Walker & Bliss, 1932), a dominant pattern of atmospheric variability in the North Pacific, on the tropical Pacific either through the seasonal footprinting mechanism (Vimont, Wallace, et al., 2003; Vimont, Battisti, et al., 2003) or the trade wind charging mechanism (Anderson, 2004; Anderson et al., 2013). Following these studies, fluctuations in the boreal winter NPO-like atmospheric pattern can give rise to a boreal spring SST footprint on the North Pacific Ocean by changing the net surface heat flux. This SST footprint, which is termed the Victoria mode (VM; Bond et al., 2003; Ding, Li, Tseng, Sun, et al., 2015) or North Pacific meridional mode (Chang et al., 2007; Chiang & Vimont, 2004), then persists

until boreal summer and can subsequently force the overlying atmosphere, resulting in surface zonal winds or subsurface temperature anomalies over the equatorial Pacific that are conducive to the initiation of subsequent ENSO events.

The extratropical South Pacific Ocean has also been shown to influence the onset of ENSO (Ballester et al., 2011; Ding, Li, & Tseng, 2015; Terray, 2011). Ding, Li, and Tseng (2015) found that a quadrapole SST anomaly pattern in the extratropical South Pacific triggered by the Pacific-South American (PSA)-like atmospheric variability (Mo & Higgins, 1998)—known as the South Pacific quadrapole (SPQ) mode—precedes the ENSO signal by approximately three seasons. The SPQ influence on ENSO shares a similar forcing mechanism with the VM influence on ENSO. That is, air-sea coupling processes associated with the SPQ, which closely resemble the seasonal footprinting mechanism or trade wind charging mechanism, play an important role in initiating ENSO. In addition, the SST anomaly signature of the SPQ in the subtropical South Pacific resembles the South Pacific meridional mode pattern (Zhang, Clement, et al., 2014; Zhang, Deser, et al., 2014), which could propagate through the wind-evaporation-SST feedback (Xie & Philander, 1994) to the equatorial Pacific, thus leading to ENSO-like variability.

Given that both the extratropical North and South Pacific oceans exert an influence on ENSO, it seems worthwhile to quantify their relative importance in initiating ENSO. However, the relative contributions of the VM and SPQ SST forcing on ENSO have not been widely discussed in the literature. Using linear inverse models, Capotondi and Sardeshmukh (2015) examined the relative role of several SST and subsurface temperature precursors in triggering different types of ENSO events, but they mainly discussed the relative role of tropical/subtropical precursors in triggering ENSO events rather than that of extratropical precursors. Ding, Li, and Tseng (2015) presented a preliminary comparison of the influence of the VM and SPQ on ENSO, based on observational data. However, no detailed study of the relative contributions of the VM and SPQ to ENSO based on observations has been published. In addition, the relatively short observational records with a mixture of various climate variabilities also pose a challenge of identifying the relative role of the VM and SPQ in initiating ENSO. To address this issue, this study uses both observations and coupled general circulation models (CGCMs) to further assess the relative contributions of the VM and SPQ SST forcing to the development of ENSO.

The rest of the paper is organized as follows. Section 2 describes the various data sets, models, and indices employed in this study. Section 3 reveals the relative contributions of the VM and SPQ to ENSO in observations. The results from numerical simulations are analyzed in section 4. A further discussion regarding the joint effect of the VM and SPQ on ENSO is given in section 5. Finally, section 6 summarizes our major findings.

2. Data and Model Descriptions

2.1. Observational Data Sets

Atmospheric fields including surface winds were obtained from the National Centers for Environmental Prediction-National Center for Atmospheric Research (NCEP-NCAR) reanalysis data set for 1948 to 2017 (Kalnay et al., 1996). Monthly global SST data for the same period are from the U.K. Met Office Hadley Center Sea Ice and Sea Surface Temperature data set (HadISST3; Rayner et al., 2006) and the National Oceanic and Atmospheric Administration (NOAA) Extended Reconstructed SST, version 4 (ERSSTv4; Smith et al., 2008).

Monthly anomalies for all variables were computed by subtracting the 1981–2010 climatological means for each month. We used a 9-year high-pass filter to remove interdecadal variability and focus on the interannual time scales. We used correlation, regression, and composite analyses to examine the relative contributions of the VM and SPQ to ENSO. The statistical significance of correlation, regression, and composite analyses was determined based on a two-tailed Student's t test.

2.2. Numerical Models

The CGCM used in the study is the Community Earth System Model version 1.2.2 (hereafter CESM). The CESM is a state-of-the-art, fully coupled, global climate model developed at NCAR to simulate the whole Earth system (Hurrell et al., 2013). CESM consists of atmospheric, ocean, ice, land surface, and other components. Its atmospheric component is the Community Atmosphere Model version 5 (CAM5), with a

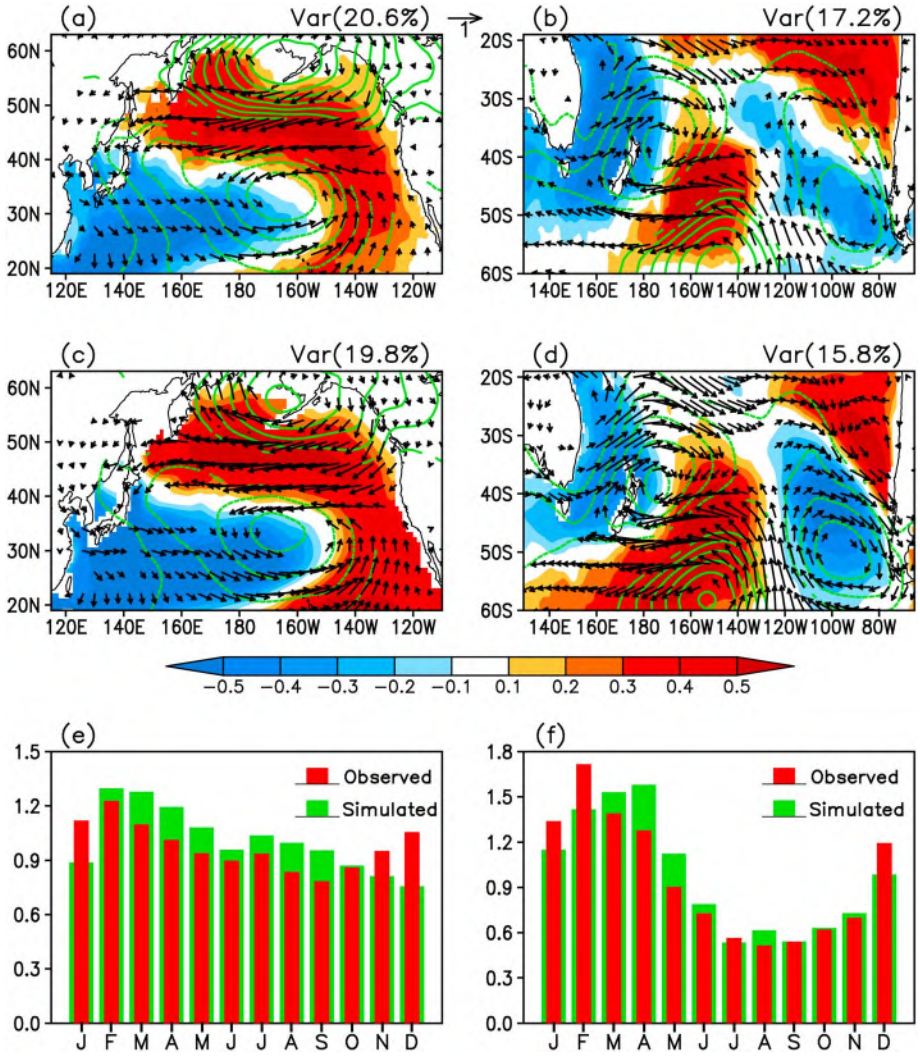

Figure 1. (a) The observed VM SST (°C; shaded) pattern and regressions of SLP (mbar; contours) and surface wind (m/s; vectors) anomalies onto the VM index. (b) The observed SPQ SST pattern and regressions of SLP and surface wind anomalies onto the SPQ index. (c, d) As in (a, b) but for the simulated SST, SLP, and surface wind patterns associated with the VM and SPQ in the CESM CTRL run. (e) Seasonal variations of the standard deviation of the observed VM index and the simulated VM index in the CESM CTRL run. (f) Seasonal variations of the standard deviation of the observed SPQ index and the simulated SPQ index in the CESM CTRL run. CESM = Community Earth System Model version 1.2.2; SLsea level pressure; SPQ = South Pacific quadrapole; SST = sea surface temperature; VM = Victoria mode.

horizontal resolution of about 1° (1.25° × 0.9°) and 30 layers in the vertical, and its ocean component is the Parallel Ocean Program version 2, with a similar horizontal resolution and 60 layers in the vertical. The land and sea ice model of CESM are the Community Land Model version 4) and Los Alamos Sea Ice Model version 4 (CICE4). The control CESM simulation is initialized from the CESM Large Ensemble (30 members) control simulation run in 1920. We integrate for 80 years from 1921 to 2000 (denoted as the CTRL run) using the 20th-century historical forcing. Several different sensitivity experiments are performed from 1921 to 2000 to explore the relative role of VM and SPQ.

2.3. VM and SPQ Indices

The first empirical orthogonal function mode of monthly SST anomalies over the North Pacific poleward of 20°N is known as the Pacific Decadal Oscillation (Mantua et al., 1997; Zhang et al., 1997), while the first empirical orthogonal function mode of monthly SST anomalies over the South Pacific poleward of 20°S represents an ENSO-like SST pattern over the South Pacific (Ding, Li, & Tseng, 2015). The VM pattern is

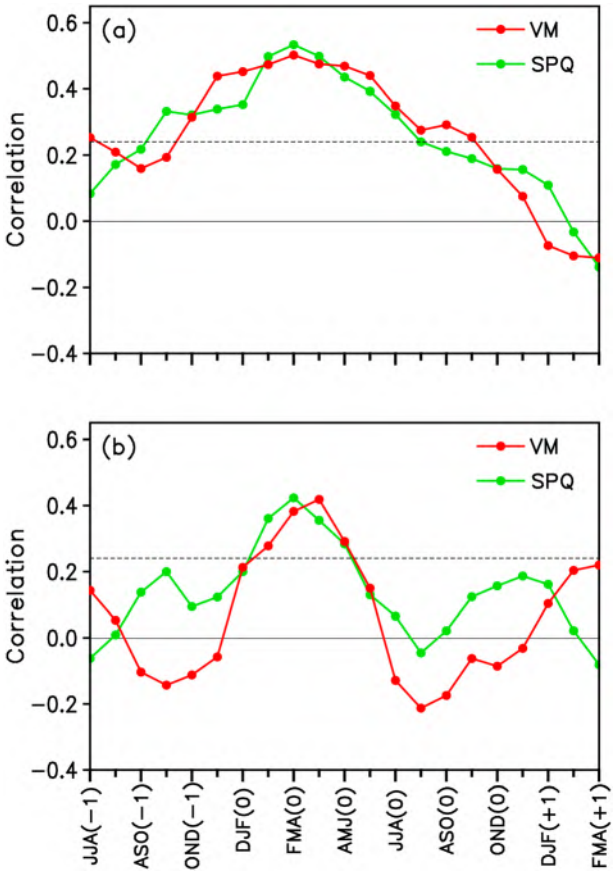

Figure 2. (a) Lead-lag correlations of the boreal winter (DJF-averaged) Niño3.4 index with 3-month-averaged VM and SPQ indices for the observations. The year in which the VM and SPQ peak in FMA is denoted as year(0) and the preceding and following years as year(−1) and year(+1). The horizontal dashed line shows the 95% confidence level. (b) As in (a) but for the Community Earth System Model version 1.2.2 CTRL run. FMA = February–April; AMJ = April–June; JJA = June–August; ASO = August–October; OND = October–December; DJF = December–February; SPQ = South Pacific quadrapole; VM = Victoria mode.

defined as the second empirical orthogonal function mode (EOF2) of monthly SST anomalies over the North Pacific poleward of 20°N (Bond et al., 2003; Ding, Li, Tseng, Sun, et al., 2015), and the SPQ pattern is defined as the EOF2 of monthly SST anomalies over the South Pacific poleward of 20°S (Ding, Li, & Tseng, 2015; Qin et al., 2018). The second principal component (PC2) time series associated with the VM (SPQ) pattern is normalized to have unit amplitude and is then defined as the VM (SPQ) index. Figures 1a and 1b show the EOF2 of North and South Pacific SST anomalies for 1948–2017 derived from the HadISST data, respectively. The VM and SPQ patterns explain 20.6% and 17.2% of the total variance, respectively, and are well separated from the remaining eigenvectors according to the criterion of North et al. (1982). The most obvious feature of the VM pattern is a tilted SST anomaly dipole structure oriented in the northeast-southwest direction over the North Pacific, with a band of positive SST anomalies extending from the Sea of Okhotsk to the northeastern North Pacific and a band of negative SST anomalies extending from the central North Pacific to the western North Pacific. The sea level pressure (SLP) anomaly pattern associated with the VM exhibits a dipole structure with opposite SLP anomalies over the midlatitude North Pacific and the high-latitude North Pacific (Figure 1a), which resembles the NPO pattern (Walker & Bliss, 1932). The prominent feature of the SPQ pattern is a quadrapole-like SST anomaly structure over the South Pacific, with centers over the Tasman Sea off the southeast coast of Australia, the Ross Sea, the Bellingshausen Sea, and the west coast of South America. The SPQ is related to SLP variability over the South Pacific with a zonal wave number-3 structure (Figure 1b), which resembles the PSA pattern (Mo & Higgins, 1998).

Both the VM and SPQ reach their peak around boreal spring (February–April [FMA]; Figures 1e and 1f), consistent with Ding, Li, Tseng, Sun, et al. (2015), Ding, Li, and Tseng, (2015). Lead-lag correlations of the December–February (DJF)-averaged Niño3.4 index with 3-month-averaged VM and SPQ indices indicate that their peak correlations occur around boreal spring (FMA) prior to the boreal winter peak of ENSO for both the observations and CESM CTRL run (Figures 2a and 2b). Therefore, we used the FMA-averaged VM and SPQ indices as representative of VM/SPQ variability to compare their relationships with ENSO in the observations as well as in the CESM. Figure 3a shows time series of the observed FMA-averaged VM and SPQ indices for the period 1948–2017. The correlation between the FMA-averaged VM and SPQ indices is 0.22 (not significant at the 95% confidence level; see also Figure 4a). This indicates that VM variability is relatively independent of SPQ variability, consistent with the findings of Ding, Li, and Tseng (2015). According to the FMA-averaged VM and SPQ indices (Figure 3a), a strongly positive or negative VM (SPQ) event is defined as a year in which the FMA-averaged VM (SPQ) index exceeds one positive or negative standard deviation of its 1948–2017 time series (Table 1). Note that only 6 of the 26 VM events occurred simultaneously with SPQ events, lending support to the view that the VM is relatively independent from the SPQ.

3. Observational Analysis

The evolution of 3-month-averaged SST and surface wind anomalies regressed on the FMA-averaged VM and SPQ indices derived from the HadISST data is shown in Figure 5. The figure indicates that both the boreal spring VM and SPQ induce significant westerly anomalies in the western equatorial Pacific and positive SST anomalies in the central-eastern equatorial Pacific during the following boreal summer, which are sustained and further developed by the Bjerknes feedback in the tropical Pacific during subsequent seasons, as shown previously by Ding, Li, Tseng, Sun, et al. (2015), Ding, Li, and Tseng, (2015). We note that the

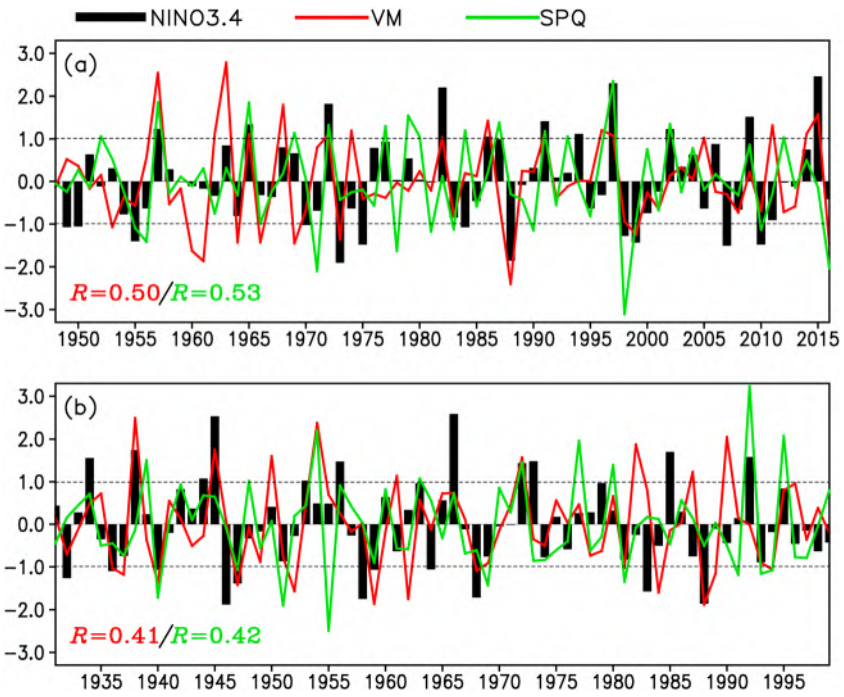

Figure 3. (a) Time series of the observed FMA-averaged VM and SPQ indices overlaid with the following boreal winter (December to February-averaged) Niño3.4 index for 1948–2017. (b) As in (a), but for the time series of the simulated VM, SPQ, and Niño3.4 indices in the Community Earth System Model version 1.2.2 CTRL run for 1931–2000. In (a) and (b), the correlations of the FMA-averaged VM and SPQ indices with the following boreal winter Niño3.4 index are given in the lower left corner. FMA = February–April; SPQ = South Pacific quadrapole; VM = Victoria mode.

maximum warming induced by both the VM and SPQ is mostly located in the Niño3.4 region (170–120°W, 5°S to 5°N). Thus, we used the Niño3.4 index (SST averaged over [170–120°W, 5°S to 5°N]) as representative of ENSO variability to compare its linkages with the VM and SPQ.

We first compute the correlations of the boreal spring (FMA-averaged) VM and SPQ indices with the following boreal winter (DJF-averaged) Niño3.4 index for 1948–2017. The correlation between the VM and Niño3.4 indices is 0.50 (significant at the 99.9% confidence level; Figures 4b), which is slightly lower than the correlation between the SPQ and Niño3.4 indices (R = 0.53, significant at the 99.9% confidence level; Figure 4c). The difference between these two correlations is not significant at the 95% confidence level according to the Monte Carlo significance test (Anderson, 2007). Furthermore, the partial correlation technique (Spiegel, 1988) is utilized to distinguish the impacts of the VM and SPQ on ENSO. The partial correlation between the VM and Niño3.4 indices after excluding the impact of the SPQ is also similar to that between the SPQ and Niño3.4 indices after excluding the impact of the VM (0.41 and 0.43, respectively; both significant at the 99.9% confidence level). These results are consistent with those of Ding, Li, and Tseng (2015), who found that the lagged correlation between the VM and ENSO is comparable with that between the SPQ and ENSO.

We next compare the amplitudes of the VM-related and SPQ-related Niño3.4 indices using regression and composite analyses. The regression coefficient of the following boreal winter (DJF-averaged) Niño3.4 index onto the FMA-averaged VM index is very close to the regressed Niño3.4 index onto the SPQ index (0.56 and 0.55 °C, respectively; both significant at the 99.9% confidence level). The partial regression coefficient of the VM after excluding the impact of the SPQ is also similar to that of the SPQ after excluding the impact of the VM (0.39 and 0.37 °C, respectively; both significant at the 99% confidence level). Half the composite difference in the following boreal winter Niño3.4 index between positive and negative VM events is of comparable amplitude to that between positive and negative SPQ events (0.73 and 0.68 °C, respectively; both significant at the 99% confidence level). We note that although the magnitudes of the boreal winter Niño3.4 index associated with the VM and SPQ are comparable, their seasonal evolutions are somewhat different. In contrast to the Niño3.4 index associated with the VM, the Niño3.4 index associated with the SPQ indicates an earlier

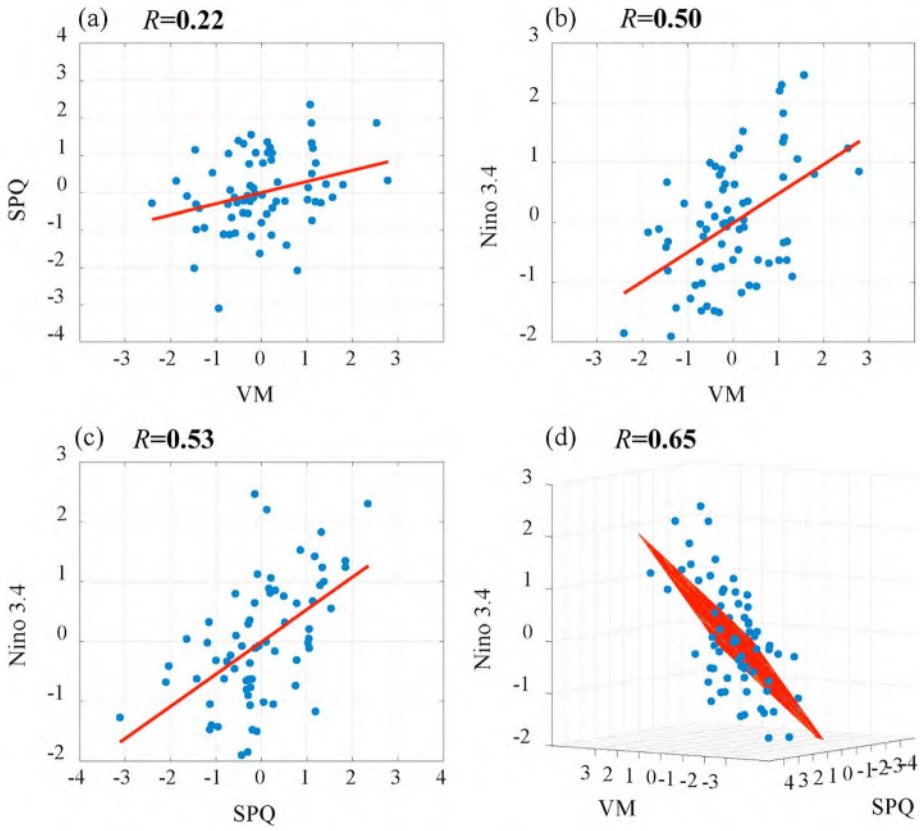

Figure 4. (a) Scatterplot with regression fitting line of the FMA-averaged VM index versus the simultaneous SPQ index. (b) As in (a), but for the FMA-averaged VM index versus the following boreal winter (DJF-averaged) Niño3.4 index. (c) As in (a), but for the FMA-averaged SPQ index versus the following boreal winter Niño3.4 index. (d) Scatterplot with regression fitting plane of the FMA-averaged VM and SPQ indices versus the following boreal winter Niño3.4 index. SPQ = South Pacific quadrapole; VM = Victoria mode.

transition from the negative to positive phase during boreal spring, followed by a quicker decay after it reaches its peak during boreal winter (Figure 6).

Furthermore, we make a comparison of the percentages of positive (negative) VM and SPQ events that are followed by a strong or moderate El Niño (La Niña) event. A strong (moderate) El Niño or La Niña event is defined by a boreal winter (DJF) Niño3.4 index greater than 1.0 (0.5–1.0) positive standard deviation or less than 1.0 (0.5–1.0) negative standard deviation. About 42% of the VM events (11 out of 26 events) were followed by a strong ENSO event (Table 2). Similarly, around 42% of the SPQ events (10 out of 24 events) were followed by a strong ENSO event. In addition, 4 out of 26 VM events (~15%) were followed by a moderate ENSO event, whereas 6 out of 25 SPQ events (~24%) were followed by a moderate ENSO event. In general,

Table 1
Years of Positive or Negative VM and SPQ Events for the Period 1948–2017

Event	Year
Positive VM	**1957**, 1962, 1963, **1965**, 1968, **1972**, 1974, 1982, 1986, **1991**, 1996, **1997**, 2005, 2011, 2014, 2015
Negative VM	1953, 1960, 1961, 1964, 1966, 1969, 1973, 1988, 1999, **2016**
Positive SPQ	**1957**, **1965**, 1969, **1972**, 1977, 1979, 1980, 1984, 1987, **1991**, 1993, **1997**, 2002, 2012
Negative SPQ	1955, 1956, 1971, 1978, 1981, 1983, 1990, 1998, 2010, **2016**

Note. Positive (negative) VM events that occurred simultaneously with the SPQ events are highlighted in bold red (blue). SPQ = South Pacific quadrapole; VM = Victoria mode.

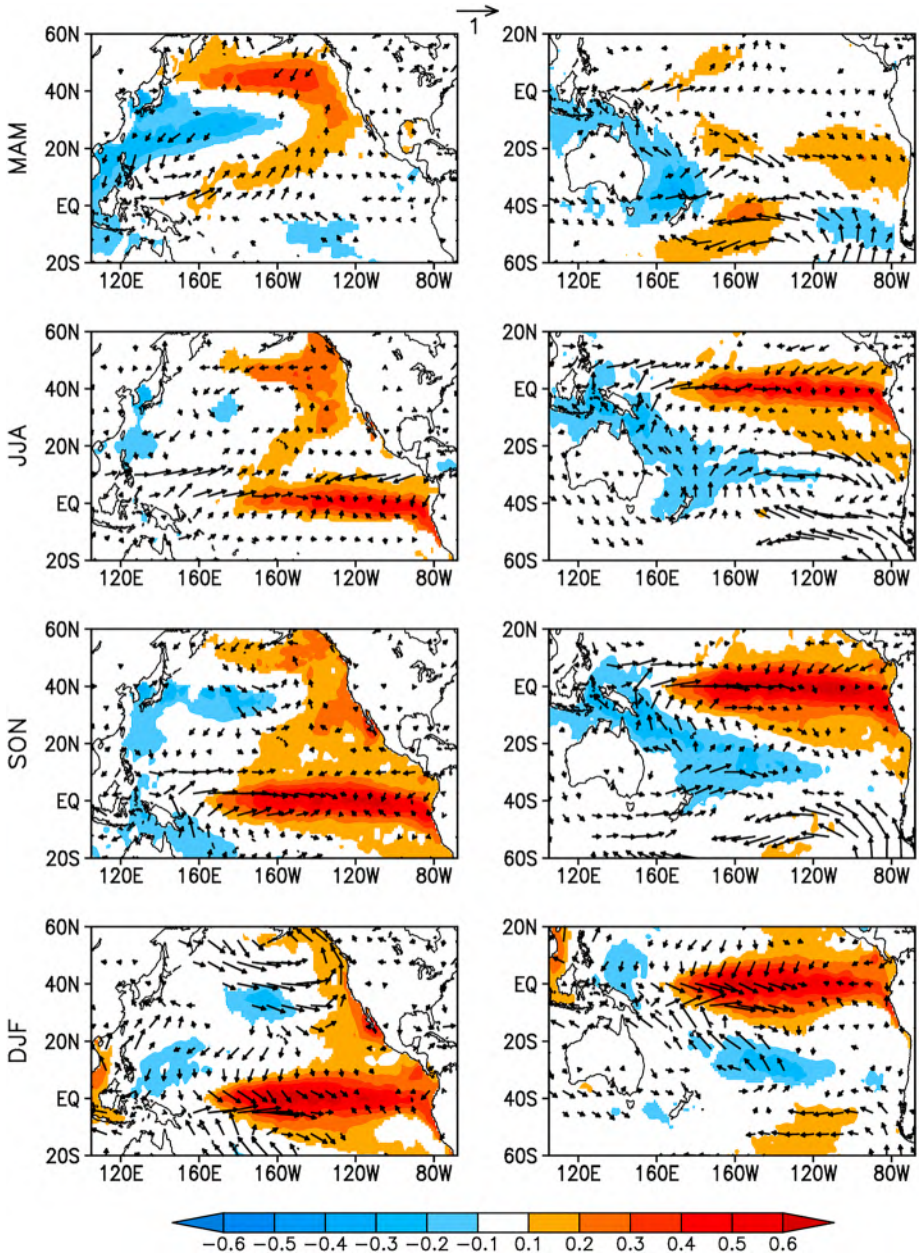

Figure 5. Regressions of the observed 3-month averaged sea surface temperature (°C; shaded) and surface wind anomalies (m/s; vectors) onto the February to April-averaged VM (left panel) and SPQ (right panel) indices for several lead times (MAM, JJA, SON, and DJF). Positive (red) and negative (blue) sea surface temperature anomalies, significant at the 95% confidence level, are shaded. Only surface wind vectors significant at the 95% confidence level are shown. JJA = June–August; SON = September–November; DJF = December–February; MAM = March–May.

the percentages of VM and SPQ events that were followed by strong and moderate ENSO events are similar. Note that around 42% of VM or SPQ events were followed by a strong ENSO event, indicative of the importance of the North and South Pacific extratropical forcings in influencing ENSO.

The comparisons presented above are summarized in Figure 7. The relationships of the VM and SPQ with ENSO are consistent between HadISST and ERSST (the left and right panels of Figure 7, respectively), indicating that the results are not sensitive to the choice of data set. These results from observational studies suggest that the effects of the VM and SPQ on ENSO are generally comparable, and the VM plays an important role, similar to the SPQ, in the development of subsequent ENSO events.

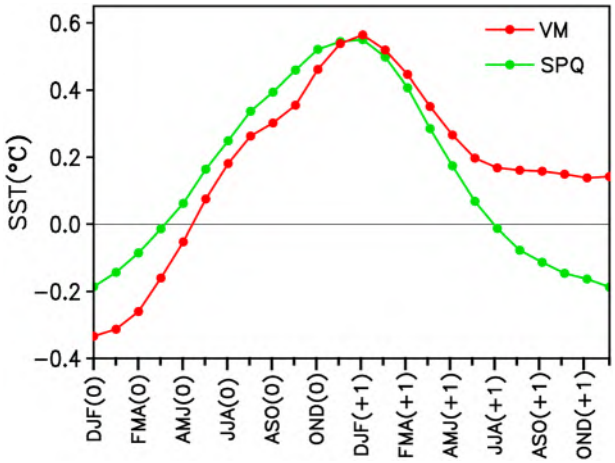

Figure 6. Lead-lag regression coefficients of the 3-month-averaged Niño3.4 index on the FMA-averaged VM and SPQ indices derived from the Hadley Center Sea Ice and Sea Surface Temperature data. The year in which the VM and SPQ peak in FMA is denoted as year(0) and the following year as year(+1). FMA = February–April; AMJ = April–June; JJA = June–August; ASO = August–October; OND = October–December; DJF = December–February; SPQ = South Pacific quadrapole; VM = Victoria mode; SST = sea surface temperature.

4. Numerical Experiments

To further explore the relative contributions of the VM and SPQ to ENSO, we performed numerical sensitivity experiments with the CESM by imposing the VM-related (SPQ-related) SST anomalies only over the North Pacific poleward of 10°N (over the South Pacific poleward of 10°S; Figure 8). The VM-related (SPQ-related) SST anomalies are obtained from regressions of the FMA-averaged SST anomalies onto the concurrent VM (SPQ) index based on the HadISST data. It should be noted that although the VM (SPQ) mode is defined as the EOF2 of SST anomalies over the North Pacific poleward of 20°N (over the South Pacific poleward of 20°S), its related SST anomalies can extend into the subtropical North (South) Pacific (see the MAM season of Figure 5). These subtropical SST anomalies associated with the VM (SPQ) could be considered as a part of the VM-related (SPQ-related) SST anomaly pattern in the North Pacific (in the South Pacific), and they may play an important role in linking the VM/SPQ to ENSO Ding, Li, Tseng, Sun, et al. (2015), Ding, Li, and Tseng, (2015). Therefore, we superimposed the VM-related or SPQ-related SST anomaly pattern poleward of 10° rather than poleward of 20°.

The sensitivity experiment superimposes the VM-related (or SPQ-related) SST anomalies (Figure 8) to the oceanic SST patterns in the coupler only in the FMA season every year so that the enhanced SST can be feed into the CAM5 and represents the enhanced roles of the boreal spring VM and SPQ. We note that the oceanic SST climatology is not significantly changed (figures not shown) since only the atmospheric model CAM5 feels the additional SST patterns and then feedbacks back to the ocean through the surface heat flux. Therefore, we do not perform further restoring to the model climatology. The numerical experiment with the additional VM-related SST anomalies is denoted as the NP run, while the experiment with the additional SPQ-related SST anomalies is denoted as the SP run. In the NP (SP) run, the ocean-atmosphere coupling is not influenced except the imposed regions during the FMA season. Similar to the CESM CTRL run described in section 2.2, each experiment was also integrated for 80 years from 1921, and the last 70 years were used in the analysis. The difference between the NP and CTRL runs reveals the contribution of the VM SST forcing to ENSO, while the difference between the SP and CTRL runs reveals the contribution of the SPQ SST forcing.

Before proceeding to an investigation of the relative contribution of the VM and SPQ to ENSO in the CESM, it is necessary to evaluate the model's performance in simulating the VM and SPQ patterns and their effects on tropical Pacific SST variability. The simulations of the EOF2 of North and South Pacific SST anomalies derived from the CTRL run are shown in Figures 1c and 1d, respectively. The EOF2 modes of North and South Pacific SST anomalies explain slightly smaller variances within the simulations than within the observations (19.8% and 15.8% in the simulations compared with 20.6% and 17.2% in the observations). The simulated EOF2 of North Pacific SST anomalies shows a dipole structure oriented in the northeast-southwest direction similar to the observations. The simulated EOF2 of South Pacific SST anomalies also resembles

Table 2
Classification of Years in Which Positive or Negative VM and SPQ Events Were or Were Not Followed by a Strong El Niño or La Niña Event for 1948–2017

	Strong El Niño	No strong El Niño or La Niña	Strong La Niña
Positive VM	1957, 1965, 1972, 1982, 1986, 1991, 1997, 2005, 2015	1962, 1963, 1968, 1974, 1996, 2011, 2014	
Negative VM		1953, 1960, 1961, 1964, 1966, 1969, 2016	1973, 1988, 1999
Positive SPQ	1957, 1965, 1972, 1991, 1997, 2002	1969, 1977, 1979, 1980, 1984, 1987, 1993, 2012	
Negative SPQ		1956, 1971, 1978, 1981, 1990, 2016	1955, 1983, 1998, 2010

Note. SPQ = South Pacific quadrapole; VM = Victoria mode.

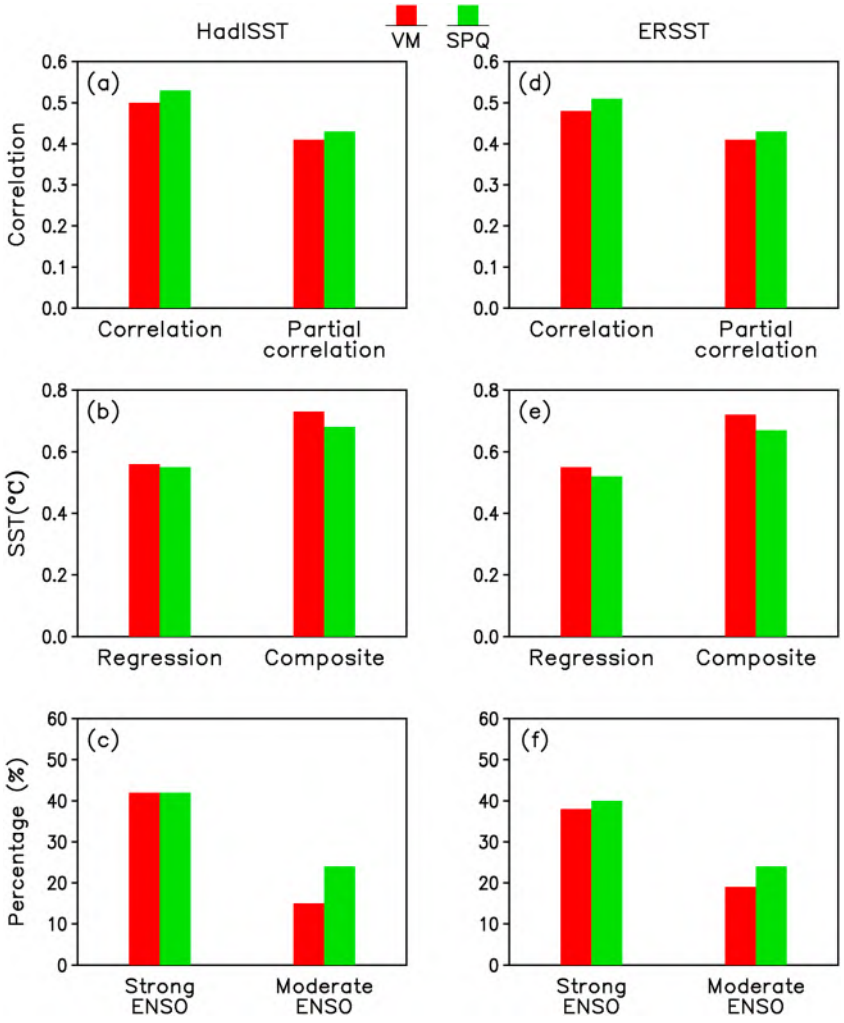

Figure 7. (a) Correlations and partial correlations of the FMA-averaged VM and SPQ indices with the following boreal winter (DJF-averaged) Niño3.4 index. (b) The regression coefficients of the DJF-averaged Niño3.4 index onto the FMA-averaged VM index and half the composite difference in the DJF-averaged Niño3.4 index between positive and negative VM (SPQ) events. (c) Percentages of positive (negative) VM and SPQ events that are followed by a strong or moderate El Niño (La Niña) event. (d–f) Same as (a–c), respectively, but calculated using ERSST data. In (a–f), the red and green bars are for the VM and SPQ, respectively. ENSO = El Niño–Southern Oscillation; ERSST = Extended Reconstructed SST; HadISST = Hadley Center Sea Ice and Sea Surface Temperature; SST = sea surface temperature; FMA = February–April; DJF = December–February; SPQ = South Pacific quadrapole; VM = Victoria mode.

the SPQ pattern in the observations, with a quadrapole-like SST anomaly structure over the South Pacific. The pattern correlations between the simulated and observed VM SST patterns and between the simulated and observed SPQ SST patterns reach 0.88 and 0.85, respectively. The simulated VM and SPQ patterns are related to the NPO-like and PSA-like atmospheric patterns (Figures 1c and 1d), respectively, consistent with the observations. The temporal characteristics of the simulated VM and SPQ indices (Figures 1e and 1f) also show similarities to the observations: The seasonal variation of the standard deviation of both indices peaks around the FMA season. These results indicate that CESM can well reproduce the temporal and spatial features of the VM and SPQ modes.

The evolutions of 3-month-averaged SST and surface wind anomalies regressed on the FMA-averaged VM and SPQ indices were also evaluated for the CTRL run (Figure 9). The CTRL run realistically reproduces the equatorward propagation of off-equatorial SST and surface wind anomalies associated with the VM and SPQ. Some key characteristics of the processes involved in the influence of the

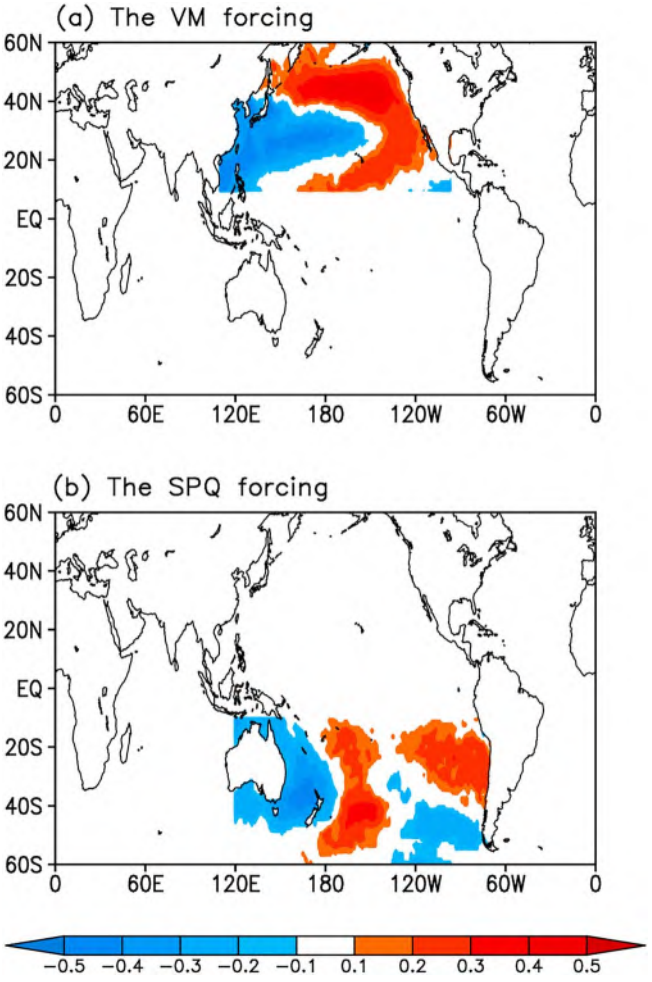

Figure 8. Prescribed SST anomalies (°C; shaded) during the FMA season respectively for the (a) NP and (b) SP experiments, which are obtained from regressions of the FMA-averaged SST anomalies onto the concurrent VM/SPQ index based on the HadISST data. SPQ = South Pacific quadrapole; VM = Victoria mode.

VM and SPQ on ENSO, such as significant SST anomalies in the subtropical North/South Pacific persisting from boreal spring to summer, pronounced westerly anomalies in the western equatorial Pacific from boreal summer, and the associated positive SST anomalies in the central-eastern equatorial Pacific, are well simulated. The maximum warming center during boreal winter associated the VM, and SPQ is located over the Niño3.4 region between 170° and 120°W, consistent with the observations. The major differences between the CTRL run and the observations are that the simulated westerly anomalies in the western equatorial Pacific in boreal summer and the simulated Niño3.4 index in boreal winter are slightly weaker than those in the observations. Despite these differences, the correlation between the FMA-averaged VM index and the following boreal winter Niño3.4 index is comparable to that between the SPQ index and the Niño3.4 index three seasons later in the CTRL run (0.41 and 0.42, respectively; see Figure 3b), and the simulated Niño3.4 index in the boreal winter associated with the VM is of comparable amplitude to that associated with the SPQ (0.46°C and 0.45°C, respectively), which resemble the observations.

The results from the CTRL run presented above show that the simulated responses of ENSO resulting from the VM and SPQ SST forcing are relatively realistic. This gives us confidence to further investigate the relative contribution of the VM and SPQ to ENSO through comparing the results of the NP and SP runs. The differences in the seasonal evolution of SST and surface wind anomalies between the NP and CTRL runs are shown in Figure 10 (left panel). During boreal spring, significant positive SST anomalies associated with the VM extend from the northeastern Pacific to the tropical central Pacific. These SST anomalies generate the anomalous westerlies in the western equatorial Pacific by modifying the SST anomaly gradient. Driven by these equatorial anomalous westerlies, the El Niño signal starts to emerge in the eastern equatorial Pacific from boreal summer and further develops during subsequent seasons. These results from the NP run confirm the role of the VM SST forcing as a trigger of ENSO.

The differences in the seasonal evolution of SST and surface wind anomalies between the SP and CTRL runs are shown in Figure 10 (right panel). During boreal spring, both negative SST anomalies off the east coast of Australia and positive SST anomalies along the west coast of South America associated with the SPQ extend northwestward toward the western and central-eastern equatorial Pacific, respectively, leading to a weakened zonal SST gradient across the western to eastern equatorial Pacific. In turn, this gradient induces westerly anomalies in the western equatorial Pacific during boreal summer that are conducive to initiating an El Niño pattern during subsequent seasons via ocean-atmosphere coupling in the tropics. Consistently, the results from the SP run show that the SPQ SST forcing during boreal spring favors El Niño signals during the subsequent boreal winter.

The above idealized numerical experiments show that both the boreal spring VM and SPQ SST forcing contribute to the subsequent development of ENSO events. To reveal the relative contribution of the VM and SPQ SST forcing, we compare the seasonal evolutions of the Niño3.4 index from boreal spring to winter simulated by the NP and SP runs (Figure 11a). The Niño3.4 index in both runs intensifies during boreal summer and fall and peaks during boreal winter, lagging the VM/SPQ SST forcing during the FMA season by three seasons. The boreal winter Niño3.4 index in the NP run has amplitude comparable to that in the SP run. In addition, CESM tends to simulate a higher probability of an El Niño state in both the NP and SP runs under VM or SPQ SST forcing. Both the NP and SP runs have a higher

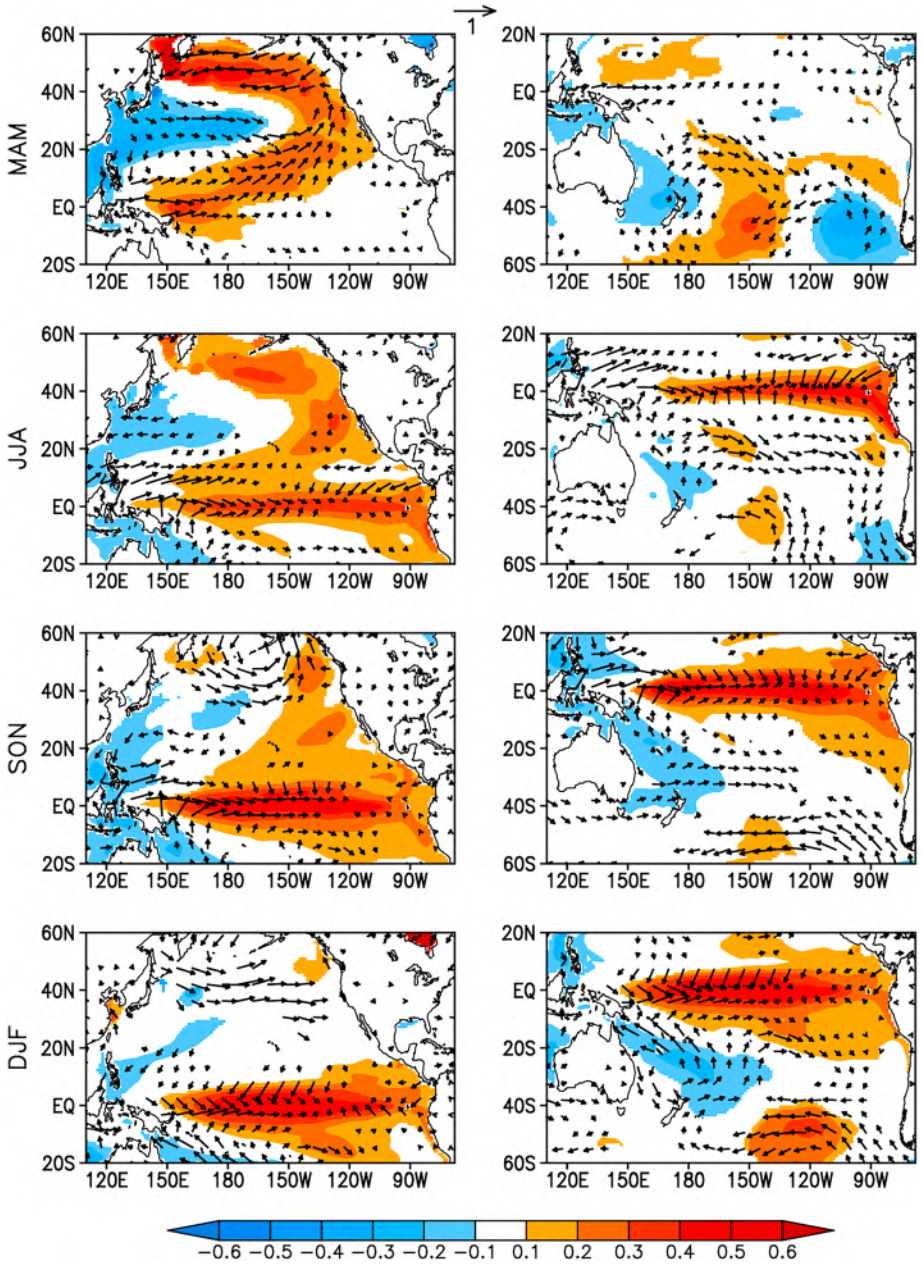

Figure 9. The evolutions of 3-month-averaged sea surface temperature (°C; shaded) and surface wind anomalies (m/s; vectors) regressed on the February to April-averaged Victoria mode (left panel) and South Pacific quadrapole (right panel) indices in the Community Earth System Model CTRL run for several lead times (MAM, JJA, SON, and DJF). Positive (red) and negative (blue) sea surface temperature anomalies, significant at the 95% confidence level, are shaded. Only surface wind vectors significant at the 95% confidence level are shown. JJA = June–August; SON = September–November; DJF = December–February; MAM = March–May.

probability of strong and moderate El Niño events compared with the CTRL run (Figure 11b). Here strong or moderate El Niño/La Niña events in the NP and SP runs follow the same definitions as in the observations. The probability of a strong El Niño in the NP run is similar to that in the SP run (32% and 30%, respectively). These results are consistent with those from the observational analysis, thereby supporting the conclusion that the North and South Pacific SST forcings have similar levels of importance to ENSO.

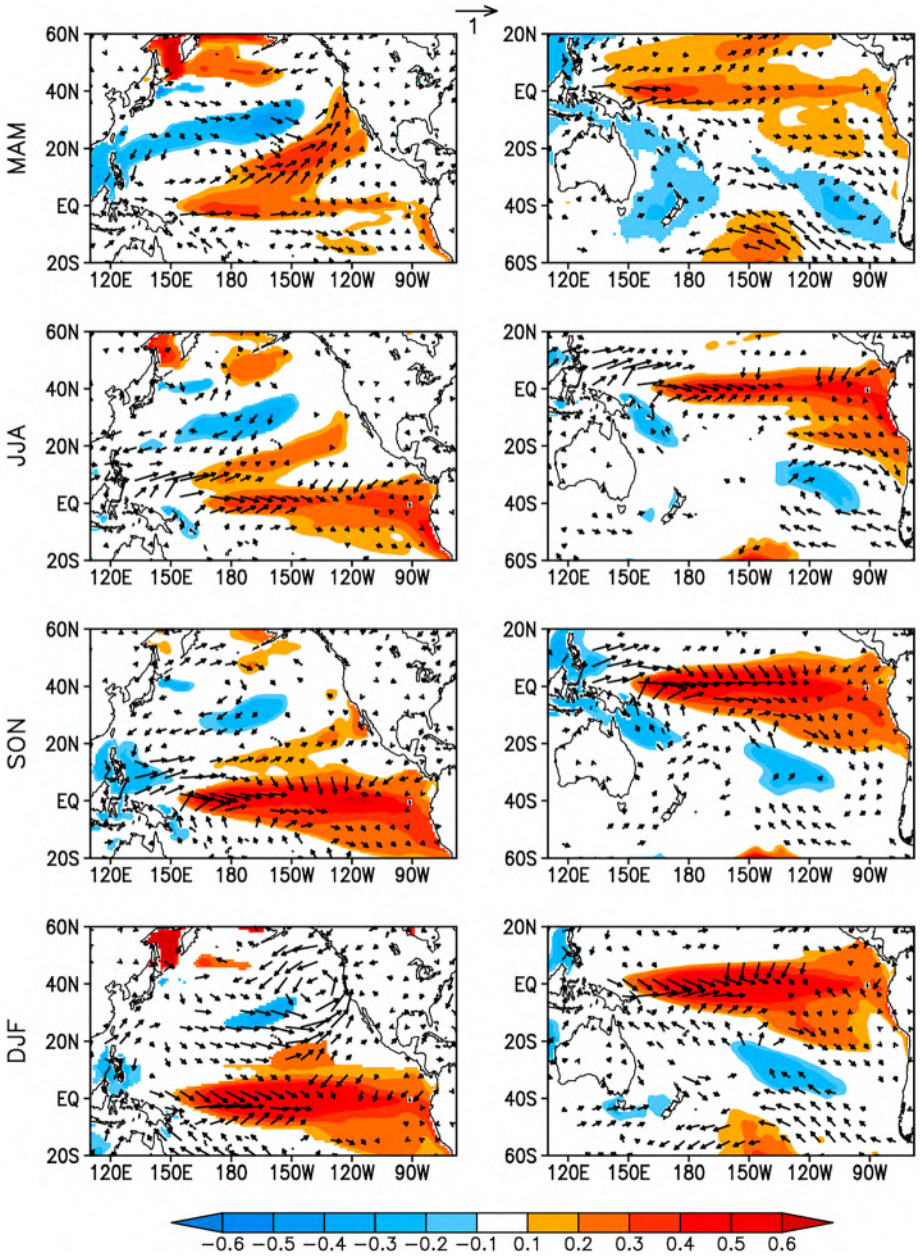

Figure 10. The differences of the 3-month-averaged SST (°C; shaded) and surface wind (m/s; vectors) anomalies between the NP and CTRL runs (left panel) and between the SP and CTRL runs (right panel). Only sea surface temperature and surface wind anomalies significant at the 95% confidence level are shown. JJA = June–August; SON = September–November; DJF = December–February; MAM = March–May.

5. Discussion

Although the majority of current CGCMs reproduce an ENSO-like dominant mode of tropical Pacific interannual SST variability, the specific properties (amplitude, frequency, and pattern) of ENSO are highly model dependent (Latif et al., 2001). Furthermore, models differ widely in their responses to the North and South Pacific SST forcing, making the estimation of the relative contributions of the VM and SPQ SST forcing to ENSO somewhat uncertain. It follows that the results from the ideal experiments in this study may be model dependent and therefore should be compared with those from other CGCMs in future research.

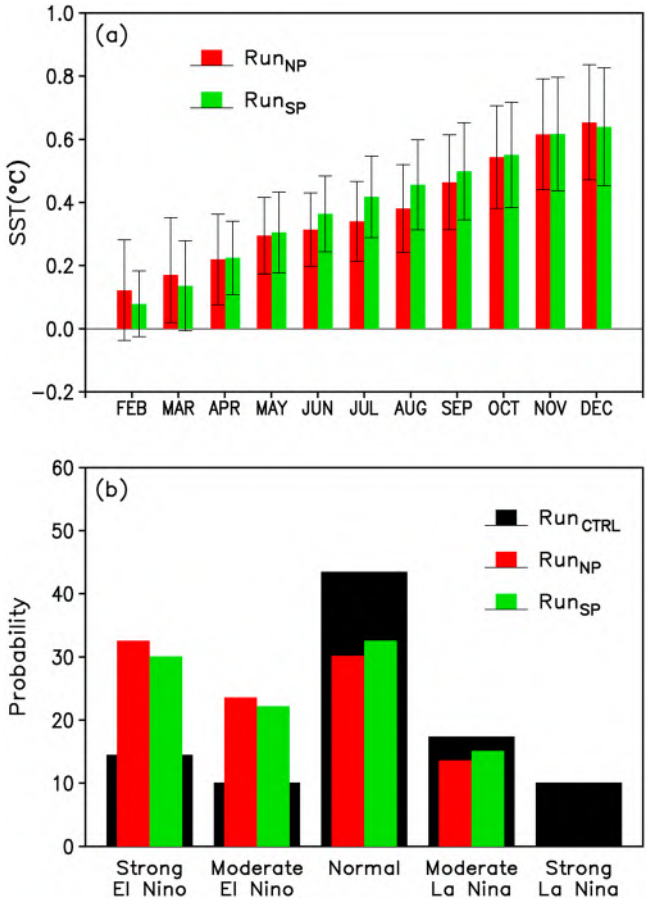

Figure 11. (a) The difference in the Niño3.4 index from February to December between the NP and CTRL runs and between the SP and CTRL runs. Error bars indicate the 95% confidence intervals. (b) Probability distributions of strong, moderate, and normal El Niño–Southern Oscillation cases in the CTRL run, in the NP run, and in the SP run. SST = sea surface temperature.

The intensities of the VM and SPQ are not constant but exhibit variations on decadal time scales in observations (Ding, Li, Tseng, Sun, et al., 2015; Ding, Li, & Tseng, 2015, 2016). Moreover, the VM amplitude does not vary in phase with the SPQ amplitude. Therefore, the relative contributions of the VM and SPQ to ENSO may depend on the decadal background state. By comparing the relative contributions of the VM and SPQ to ENSO over an extended period (1948–2017), we conclude that the VM and SPQ may make comparable contributions to ENSO. However, for a shorter period the results may be different and the VM may play a more important role in developing ENSO than the SPQ or vice versa. The dependence of the relative contributions of the VM and SPQ to ENSO on the decadal background state needs to be further investigated. In addition, the VM and SPQ possesses variability ranging from interannual to decadal time scales (Ding, Li, Tseng, Sun, et al., 2015; Ding, Li, & Tseng, 2015). This study compares the influences of the VM and SPQ on tropical Pacific interannual SST variability. Further investigations are also needed to better understand the impacts of the VM and SPQ on tropical Pacific decadal SST variability.

Though the VM or SPQ forcing alone may serve a precursor to ENSO, it is more effective to consider their joint effects. Based on observational data, Ding et al. (2017) demonstrated that the VM influence on the tropical Pacific interferes or interacts with the SPQ effect, and when the two precursors have the same (opposite) sign, their impact on ENSO is much stronger (weaker). Given the joint relationship of VM and SPQ SST forcing with ENSO, it is difficult to separately quantify their individual contributions and more worthwhile to consider a combined model for prediction. Based on the observed VM and SPQ indices in boreal spring, we developed an empirical prediction model for the tropical Pacific SST anomalies in the following boreal winter at every grid point (x, y) using a multiple linear regression method:

$$\mathrm{SST}(x,y,t) = \alpha^{*}\mathrm{VM}(t) + \beta^{*}\mathrm{SPQ}(t), \quad (1)$$

where t is time in years and the time series of SST(x, y, t), VM(t), and SPQ(t) are normalized. The regression coefficients α and β at every grid point are determined through a least squares fit of the observed SST(x, y, t) to the observed VM(t), and SPQ(t), respectively. Figures 12a and 12b show the spatial distributions of α and β in the tropical Pacific derived from the HadISST data, respectively. We can see that α and β have similar amplitudes in most regions of the tropical Pacific, and the spatial pattern of α is very similar to that of β. Significant positive values of both regression coefficients are mainly located over the tropical central-eastern Pacific and significant negative values over the tropical western Pacific, which closely resembles the typical El Niño pattern.

We used model (1) to hindcast the tropical Pacific SST anomalies during boreal winter, which produces significant correlations in most regions of the tropical Pacific (Figure 12c). Furthermore, the model is assessed with a leave-one-out cross-validation procedure, which involves iteratively removing 1 year from the time series, constructing a model based on the remaining years and hindcasting for the omitted year using this model. There are some reductions in the correlations between cross-validated hindcasts and observations (compared with those in Figure 12c), but these correlations are still significant in most regions of the tropical Pacific (Figure 12d). If model (1) is used to hindcast the boreal winter Niño3.4 index based on the VM and SPQ indices of the previous spring, it yields a correlation skill of 0.65 (significant at the 99.9% confidence level; see Figure 4d). The cross-validated correlation skill of the Niño3.4 index is 0.61 (Figure 12e), which is higher than using only the SPQ or VM index to hindcast the following boreal winter Niño3.4 index (the cross-validated correlation skill is 0.47 for the VM and 0.49 for the SPQ). These results indicate that the combined VM and SPQ indices have the potential to contribute to the prediction skill of ENSO at three-season

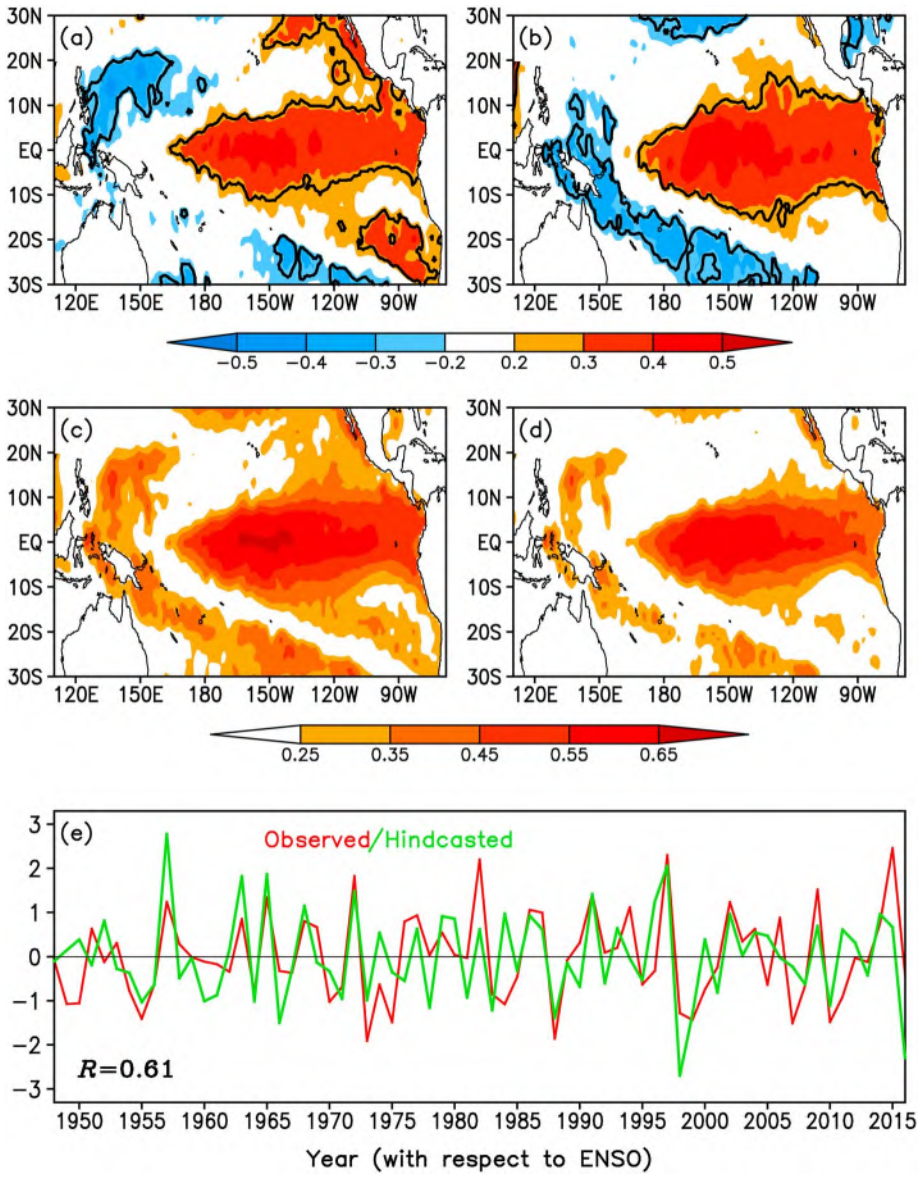

Figure 12. (a) The distribution of the regression coefficient α (shaded) determined in the empirical prediction model 1 derived from the Hadley Center Sea Ice and Sea Surface Temperature data. (b) As for (a) but for the distribution of the regression coefficient β. (c) Correlations between the observed and hindcast tropical Pacific sea surface temperature anomalies generated by the empirical prediction model 1. (d) Correlations between observations and cross-validated hindcasts of tropical Pacific sea surface temperature anomalies. In (a) and (b), the thick black contours enclose areas where the value of α or β is significantly different from 0 at the 95% confidence level. In (c) and (d), areas with correlations significant at the 95% confidence level are shaded. (e) Time series of the observed boreal winter Niño3.4 index and the cross-validated hindcasts of the boreal winter Niño3.4 index generated by empirical model (1). ENSO = El Niño–Southern Oscillation.

lead times. Further diagnosis of the real predictive use of the VM and SPQ precursors for the prediction of ENSO within a forecast framework is currently underway.

6. Conclusion

Previous studies suggest that the initiation and onset of ENSO events in the tropical Pacific can be partly associated with variations in the SST fields in the extratropical North Pacific (represented by the VM mode) as well as variations in the extratropical South Pacific (represented by the SPQ mode; Ding, Li, Tseng, Sun,

et al., 2015; Ding, Li, & Tseng, 2015; Tseng, Ding, et al., 2017). Here using observational data, we demonstrate that both VM and SPQ SST forcing during boreal spring can serve as a trigger for ENSO events. Both induce significant westerly anomalies in the western equatorial Pacific that are conducive to initiating an ENSO event in the following boreal winter. We find that the ENSO amplitudes associated with the VM and SPQ, as well as the percentages of strong ENSO events followed by the VM and SPQ events, are similar. Therefore, we conclude that the VM and SPQ may make comparable contributions to ENSO.

The relative contributions of VM and SPQ SST forcing to ENSO have been further explored in a set of numerical experiments utilizing CESM. When solely forced by the boreal spring VM-related SST anomalies in the North Pacific or the boreal spring SPQ-related SST anomalies in the South Pacific, the observed response of the tropical Pacific SST anomalies during the following boreal winter is reproduced. The simulated Niño3.4 index in the boreal winter associated with the VM is of comparable amplitude to that associated with the SPQ, supporting the idea that the VM and SPQ SST forcing have similar levels of importance to ENSO.

The important roles of the VM and SPQ in initiating ENSO have implications for prediction and general understanding of ENSO variability. Our results suggest that VM and SPQ indices may be used together to better predict tropical Pacific SST variability and ENSO events. Indeed, the high three-season lead correlation of the Niño3.4 index shown in Figure 12e is comparable to the performance of state-of-the-art CGCMs (Tseng, Hu, et al., 2017). Given that ENSO predictions are limited by the boreal spring predictability barrier (Webster & Yang, 1992), we speculate that the identification of SST anomalies associated with the VM and SPQ in the North and South Pacific, respectively, could help forecast the development of ENSO events across the boreal spring barrier. Further study is needed to investigate the role of North and South Pacific extratropical SST anomalies in affecting the predictability of ENSO.

Acknowledgments
We thank three anonymous reviewers for helpful comments and suggestions. This work was jointly supported by the National Natural Science Foundation of China (Grant 41790474) and the National Program on Global Change and Air–Sea Interaction (GASI-IPOVAI-03 and GASI-IPOVAI-06). The atmospheric reanalysis data set was obtained from NCEP-NCAR (available online at https://www.esrl.noaa.gov/psd/data/gridded/data.ncep.reanalysis.html). The ERSSTv4 data set was obtained from NOAA (available online at https://www.esrl.noaa.gov/psd/data/gridded/data.noaa.ersst.v4.html). The HadISST data set was obtained from the U.K. Met Office Hadley Centre (available online at http://www.metoffice.gov.uk/hadobs/hadsst3/). The CESM was obtained from NCAR (details of the CESM are available at http://www.cesm.ucar.edu/models/). The model output used in the figures for the experiments of this study is available at Zenodo (https://doi.org/10.5281/zenodo.2630508).

References

Alexander, M. A., Bladé, I., Newman, M., Lanzante, J. R., Lau, N. -C., & Scott, J. D. (2002). The atmospheric bridge: The influence of ENSO teleconnections on air–sea interaction over the global oceans. *Journal of Climate*, *15*(16), 2205–2231. https://doi.org/10.1175/1520-0442(2002)015<2205:TABTIO>2.0.CO;2

Anderson, B. T. (2004). Investigation of a large-scale mode of ocean–atmosphere variability and its relation to tropical Pacific sea surface temperature anomalies. *Journal of Climate*, *17*(20), 4089–4098. https://doi.org/10.1175/1520-0442(2004)017<4089:IOALMO>2.0.CO;2

Anderson, B. T. (2007). On the joint role of subtropical atmospheric variability and equatorial subsurface heat content anomalies in initiating the onset of ENSO events. *Journal of Climate*, *20*(8), 1593–1599. https://doi.org/10.1175/JCLI4075.1

Anderson, B. T., Perez, R. C., & Karspeck, A. (2013). Triggering of El Niño onset through trade wind–induced charging of the equatorial Pacific. *Geophysical Research Letters*, *40*, 1212–1216. https://doi.org/10.1002/grl.50200

Ballester, J., Rodríguez-Arias, M. À., & Rodó, X. (2011). A new extratropical tracer describing the role of the western Pacific in the onset of El Niño: Implications for ENSO understanding and forecasting. *Journal of Climate*, *24*(5), 1425–1437. https://doi.org/10.1175/2010JCLI3619.1

Bjerknes, J. (1969). Atmospheric teleconnections from the equatorial Pacific. *Monthly Weather Review*, *97*(3), 163–172. https://doi.org/10.1175/1520-0493(1969)097<0163:ATFTEP>2.3.CO;2

Bond, N. A., Overland, J. E., Spillane, M., & Stabeno, P. (2003). Recent shifts in the state of the North Pacific. *Geophysical Research Letters*, *30*(23), 2183. https://doi.org/10.1029/2003GL018597

Boschat, G., Terray, P., & Masson, S. (2013). Extratropical forcing of ENSO. *Geophysical Research Letters*, *40*, 1605–1611. https://doi.org/10.1002/grl.50229

Capotondi, A., & Sardeshmukh, D. P. (2015). Optimal precursors of different types of ENSO events. *Geophysical Research Letters*, *42*, 9952–9960. https://doi.org/10.1002/2015GL066171

Chang, P., Zhang, L., Saravanan, R., Vimont, D. J., Chiang, J. C. H., Ji, L., et al. (2007). Pacific meridional mode and El Niño–Southern Oscillation. *Geophysical Research Letters*, *34*, L16608. https://doi.org/10.1029/2007GL030302

Chiang, J., & Vimont, D. J. (2004). Analogous Pacific and Atlantic meridional modes of tropical atmosphere–ocean variability. *Journal of Climate*, *17*(21), 4143–4158. https://doi.org/10.1175/JCLI4953.1

Ding, R. Q., Li, J. P., & Tseng, Y. H. (2015). The impact of South Pacific extratropical forcing on ENSO and comparisons with the North Pacific. *Climate Dynamics*, *44*(7-8), 2017–2034. https://doi.org/10.1007/s00382-014-2303-5

Ding, R. Q., Li, J. P., Tseng, Y. H., Sun, C., & Guo, Y. P. (2015). The Victoria mode in the North Pacific linking extratropical sea level pressure variations to ENSO. *Journal of Geophysical Research: Atmospheres*, *120*, 27–45. https://doi.org/10.1002/2014JD022221

Ding, R. Q., Li, J. P., Tseng, Y. H., Sun, C., & Xie, F. (2017). Joint impact of North and South Pacific extratropical atmospheric variability on the onset of ENSO events. *Journal of Geophysical Research: Atmospheres*, *122*, 279–298. https://doi.org/10.1002/2016JD025502

Ding, R. Q., Li, P. J., Tseng, Y. H., Ha, K. J., Zhao, S., & Lee, J. Y. (2016). Interdecadal change in the lagged relationship between the Pacific–South American pattern and ENSO. *Climate Dynamics*, *47*(9-10), 2867–2884. https://doi.org/10.1007/s00382-016-3002-1

Ham, Y. G., Kug, J. S., Park, J. Y., & Jin, F. F. (2013). Sea surface temperature in the north tropical Atlantic as a trigger for El Niño/Southern Oscillation events. *Nature Geoscience*, *6*(2), 112–116. https://doi.org/10.1038/ngeo1686

Hurrell, J. W., Holland, M. M., Gent, P. R., Ghan, S., Kay, J. E., Kushner, P. J., et al. (2013). The Community Earth System Model: A framework for collaborative research. *Bulletin of the American Meteorological Society*, *94*(9), 1339–1360. https://doi.org/10.1175/BAMS-D-12-00121.1

Jin, D., & Kirtman, B. P. (2009). Why the Southern Hemisphere ENSO responses lead ENSO? *Journal of Geophysical Research*, *114*, D23101. https://doi.org/10.1029/2009JD012657

Kalnay, E., Kanamitsu, M., Kistler, R., Collins, W., Deaven, D., Gandin, L., et al. (1996). The NCEP–NCAR 40-year reanalysis project. *Bulletin of the American Meteorological Society*, *77*(3), 437–471. https://doi.org/10.1175/1520-0477(1996)077<0437:TNYRP>2.0.CO;2

Latif, M., Sperber, K., Arblaster, J., Braconnot, P., Chen, D., Colman, A., et al. (2001). ENSIP—The El Niño simulation intercomparison project. *Climate Dynamics*, *18*(3-4), 255–276. https://doi.org/10.1007/s003820100174

Madden, R. A., & Julian, P. R. (1994). Observations of the 40–50-day tropical oscillation—A review. *Monthly Weather Review*, *122*(5), 814–837. https://doi.org/10.1175/1520-0493(1994)122<0814:OOTDTO>2.0.CO;2

Mantua, N. J., Hare, S. R., Zhang, Y., Wallace, J. M., & Francis, R. C. (1997). A Pacific interdecadal climate oscillation with impacts on salmon production. *Bulletin of the American Meteorological Society*, *78*(6), 1069–1079. https://doi.org/10.1175/1520-0477(1997)078<1069:APICOW>2.0.CO;2

McPhaden, M. J. (1999). Genesis and evolution of the 1997–98 El Niño. *Science*, *283*(5404), 950–954. https://doi.org/10.1126/science.283.5404.950

McPhaden, M. J., Bahr, F., Du Penhoat, Y., Firing, E., Hayes, S. P., Niiler, P. P., et al. (1992). The response of the western equatorial Pacific Ocean to westerly wind bursts during November 1989 to January 1990. *Journal of Geophysical Research*, *97*(C9), 14289–14303. https://doi.org/10.1029/92JC01197

Mo, K. C., & Higgins, R. W. (1998). The Pacific–South American modes and tropical convection during the Southern Hemisphere winter. *Monthly Weather Review*, *126*(6), 1581–1596. https://doi.org/10.1175/1520-0493(1998)126<1581:TPSAMA>2.0.CO;2

North, G. R., Bell, T. L., Cahalan, R. F., & Moeng, F. J. (1982). Sampling errors in the estimation of empirical orthogonal function. *Monthly Weather Review*, *110*(7), 699–706. https://doi.org/10.1175/1520-0493(1982)110<0699:SEITEO>2.0.CO;2

Qin, J. H., Zhou, L., Ding, R. Q., & Li, J. P. (2018). Influence of South Pacific quadrapole on austral winter precipitation over the SPCZ. *Environmental Research Letters*, *13*(9), 094024. https://doi.org/10.1088/1748-9326/aadd84/meta

Rayner, N. A., Brohan, P., Parker, D. E., Folland, C. K., Kennedy, J. J., Vanicek, M., et al. (2006). Improved analyses of changes and uncertainties in sea surface temperature measured in situ since the mid-nineteenth century: The HadSST2 dataset. *Journal of Climate*, *19*(3), 446–469. https://doi.org/10.1175/JCLI3637.1

Smith, T. M., Reynolds, R. W., Peterson, T. C., & Lawrimore, J. (2008). Improvements to NOAA's historical merged land-ocean surface temperature analysis (1880–2006). *Journal of Climate*, *21*(10), 2283–2296. https://doi.org/10.1175/2007JCLI2100.1

Spiegel, M. R. (1988). *Schaum's outline of theory and problems of statistics*, (2d ed.p. 504). New York: McGraw-Hill.

Terray, P. (2011). Southern Hemisphere extra-tropical forcing: A new paradigm for El Niño-Southern Oscillation. *Climate Dynamics*, *36*(11-12), 2171–2199. https://doi.org/10.1007/s00382-010-0825-z

Tseng, Y. H., Ding, R. Q., & Huang, X. M. (2017). The warm Blob in the northeast Pacific—The bridge leading to the 2015/16 El Niño. *Environmental Research Letters*, *12*(5), 054019. https://doi.org/10.1088/1748-9326/aa67c3

Tseng, Y. H., Hu, Z. Z., Ding, R. Q., & Chen, H. H. (2017). An ENSO prediction approach based on ocean conditions and ocean–atmosphere coupling. *Climate Dynamics*, *48*(5-6), 2025–2044. https://doi.org/10.1007/s00382-016-3188-2

Vimont, D. J., Battisti, D. S., & Hirst, A. C. (2003). The seasonal footprinting mechanism in the CSIRO general circulation models. *Journal of Climate*, *16*(16), 2653–2667. https://doi.org/10.1175/1520-0442(2003)016<2653:TSFMIT>2.0.CO;2

Vimont, D. J., Wallace, J. M., & Battisti, D. S. (2003). The seasonal footprinting mechanism in the Pacific: Implications for ENSO. *Journal of Climate*, *16*(16), 2668–2675. https://doi.org/10.1175/1520-0442(2003)016<2668:TSFMIT>2.0.CO;2

Walker, G. T., & Bliss, E. W. (1932). World weather V. *Memorial Royal Meteorological Society*, *4*, 53–84.

Wang, S.-Y., L'Heureux, M., & Chia, H.-H. (2012). ENSO prediction one year in advance using western North Pacific sea surface temperatures. *Geophysical Research Letters*, *39*, L05702. https://doi.org/10.1029/2012GL050909

Wang, S.-Y., L'Heureux, M., & Yoon, J.-H. (2013). Are greenhouse gases changing ENSO precursors in the western North Pacific. *Journal of Climate*, *26*(17), 6309–6322. https://doi.org/10.1175/JCLI-D-12-00360.1

Webster, P. J., & Yang, S. (1992). Monsoon and ENSO: Selectively interactive systems. *Quarterly Journal of the Royal Meteorological Society*, *118*(507), 877–926. https://doi.org/10.1002/qj.49711850705

Xie, S. -P., & Philander, S. G. H. (1994). A coupled ocean–atmosphere model of relevance to the ITCZ in the eastern Pacific. *Tellus*, *46A*, 340–350.

Zhang, H. H., Clement, A., & Di Nezio, P. (2014). The South Pacific meridional mode: A mechanism for ENSO-like variability. *Journal of Climate*, *27*(2), 769–783. https://doi.org/10.1175/JCLI-D-13-00082.1

Zhang, H. H., Deser, C., Clement, A., & Tomas, R. (2014). Equatorial signatures of the Pacific meridional modes: Dependence on mean climate state. *Geophysical Research Letters*, *41*, 568–574. https://doi.org/10.1002/2013GL058842

Zhang, Y., Wallace, J. M., & Battisti, D. S. (1997). ENSO-like interdecadal variability. *Journal of Climate*, *10*(5), 1004–1020. https://doi.org/10.1175/1520-0442(1997)010<1004:ELIV>2.0.CO;2